arXiv:1403.2782v1 [hep-ph] 12 Mar 2014

Next-to-next-to-leading order QCD corrections to light Higgs pair production via vector boson fusion in type-II two-Higgs-doublet model

Li Wei-Hua, Zhang Ren-You, Ma Wen-Gan, Guo Lei, Ling Liu-Sheng and Li Xiao-Zhou
Department of Modern Physics, University of Science and Technology
of China (USTC), Hefei, Anhui 230026, P.R.China

March 13, 2014

Abstract

We present the precision predictions on the pair production of light, CP-even Higgs in weak vector boson fusion (VBF) up to the QCD next-to-next-to-leading-order (NNLO) at hadron colliders within the CP-conserving type-II two-Higgs-doublet model (2HDM(II)) by adopting the structure function approach. We investigate the model parameter dependence, residual uncertainties from the factorization/renormalization scale, PDFs and α_s on the integrated cross section at the QCD NNLO, and find that the NNLO QCD corrections can reduce the scale uncertainty significantly. By analyzing the kinematic distributions of final Higgs bosons, we can extract the CP-even Higgs resonance via $H^0 \to h^0 h^0$ channel as a means of probing the extension of the Standard Model (SM) Higgs sector.

PACS: 14.80.Ec, 12.38.Bx, 12.60.Fr

1 Introduction

Both ATLAS and CMS collaborations at the Large Hadron Collider (LHC) have discovered a 126 GeV neutral boson whose properties are compatible with the Standard Model (SM) Higgs boson [1–3]. The nature of this particle, including its CP properties and couplings, is currently being established [3, 4]. So the next important step most probably is the quest for the origin of electroweak symmetry breaking (EWSB). To achieve this goal, measurement of the Higgs self-interactions is necessary, which is the only way to reconstruct the Higgs potential, and determine whether the new particle is the SM Higgs boson or one of an enlarged Higgs sector of new physics. Thus, it is useful to explore the implication of the current Higgs search results on models beyond the SM.

One of the simplest extensions of the SM Higgs sector is the two-Higgs-doublet model (2HDM) [5,6]. It predicts the existence of two neutral CP-even Higgs bosons (h^0 and H^0), one neutral CP-odd Higgs (A^0), and two charge Higgs bosons ($H^\pm$). In addition to their masses, two additional parameters are introduced in the theory: the ratio of the vacuum expectation values (VEVs) of the two Higgs doublets $\tan\beta$, and the mixing angle between the two CP-even Higgs fields α. There are many types of 2HDMs, each differing in the way that the two Higgs doublets couple to the fermions (for a comprehensive review, see [6]). In this paper, we only consider the 2HDM of type-II (2HDM(II)), which is designed to avoid flavor-changing couplings of the neutral Higgs bosons by one Higgs doublet coupling solely to up-type and the other to down-type fermions. And this model shares many of the features of the Higgs sector of the Minimal Supersymmetric Standard Model (MSSM).

To understand the Higgs self-interactions, the only accessible process is double Higgs production. At the LHC, the most important SM Higgs boson pair production channels have been systematically surveyed in Refs. [8]. The main processes are: (1) gluon-gluon fusion, $gg \to h^0h^0$, through heavy-quark loop, (2) vector boson fusion (VBF) $qq' \to V^*V^* \to q''q'''h^0h^0$, where vector bosons W/Z are radiated off quarks and fusion to Higgs pair, (3) top-quark pair associated Higgs boson pair production $q\overline{q}/gg \to t\bar{t}h^0h^0$, and (4) double Higgs strahlung $qq' \to h^0h^0V$, where Higgs bosons are radiated off gauge bosons. In the SM, Higgs pair production via VBF has the second largest cross section and offers a clean experimental signature of two centrally produced Higgs bosons with two hard jets in the forward/backward rapidity region. Hence, it is meaningful to investigate the properties of

trilinear Higgs self-interactions in this clean reaction. In this paper, we focus on the light CP-even Higgs pair production via VBF process $pp \to V^*V^* + 2\ jets \to h^0h^0 + 2\ jets$ within the 2HDM(II) to survey the properties of the trilinear Higgs self-couplings $\lambda_{h^0h^0h^0}$ and $\lambda_{H^0h^0h^0}$ appearing in the Higgs potential [7, 8]. In the previous research works, the VBF Higgs boson pair production process $pp \to h^0h^0 + 2\ jets$ was surveyed in the 2HDM(II) at the QCD NLO [15, 16].

Due to the smallness of the QCD interference between the two inclusive final proton remnants, the VBF single/pair Higgs production at the leading order (LO) can be viewed as a double deep-inelastic scattering (DIS) process in a very good approximation, and the production rate can be computed by adopting the well-known structure function (SF) approach. Apart from the interference effect, the SF approach can still be exactly employed at the QCD next-to-leading order (NLO) [9–11]. Recently, the SF approach was used to calculate the VBF single/pair Higgs production at hadron colliders in the SM up to the QCD next-to-next-to-leading order (NNLO) [12–14]. In this paper, we will implement the SF approach to calculate the VBF Higgs pair production in the 2HDM(II) up to the QCD NNLO, and provide not only the total cross section, but also some kinematic distributions of the final Higgs bosons.

The paper is organized as follows. In Sec.2, we give a brief introduction to the 2HDM(II). The description of the SF approach and the strategy of the QCD NNLO calculation are presented in Sec.3. In Sec.4, we give the numerical results and focus on the theoretical uncertainty and some kinematic distributions. A short summary is given in Sec.5. Finally, we present the analytic expressions for the phase space element and matrix elements of the VBF Higgs pair production processes in Appendix.

2 Two-Higgs-Doublet Model of Type-II

The 2HDM contains two scalar $SU(2)_L$ doublets, Φ_1 and Φ_2, with weak hypercharge $Y = 1$. The most general Higgs potential with $SU(2)_L \times U(1)_Y$, Z_2 and CP symmetries has the form as [5]

$$\begin{aligned} V(\Phi_1, \Phi_2) &= m_{11}^2 \Phi_1^\dagger \Phi_1 + m_{22}^2 \Phi_2^\dagger \Phi_2 + \frac{1}{2}\lambda_1 (\Phi_1^\dagger \Phi_1)^2 + \frac{1}{2}\lambda_2 (\Phi_2^\dagger \Phi_2)^2 \\ &\quad + \lambda_3 (\Phi_1^\dagger \Phi_1)(\Phi_2^\dagger \Phi_2) + \lambda_4 (\Phi_1^\dagger \Phi_2)(\Phi_2^\dagger \Phi_1) + \frac{1}{2}\lambda_5 \left[(\Phi_1^\dagger \Phi_2)^2 + \text{h.c.} \right], \end{aligned} \tag{2.1}$$

where m_{11}^2, m_{22}^2 and λ_i $(i = 1, ..., 5)$ are all real parameters, and $\Phi_{1,2}$ transform under the Z_2 discrete symmetry as

$$\Phi_1 \to \Phi_1, \qquad \Phi_2 \to -\Phi_2. \tag{2.2}$$

After EWSB, the neutral components of Φ_1 and Φ_2 acquire VEVs $v_1/\sqrt{2}$ and $v_2/\sqrt{2}$, respectively, which are determined by the vacuum conditions of

$$\begin{aligned} m_{11}^2 v_1 + \frac{1}{2}\lambda_1 v_1^3 + \frac{1}{2}\left(\lambda_3 + \lambda_4 + \lambda_5\right) v_1 v_2^2 = 0, \\ m_{22}^2 v_2 + \frac{1}{2}\lambda_2 v_2^3 + \frac{1}{2}\left(\lambda_3 + \lambda_4 + \lambda_5\right) v_2 v_1^2 = 0, \end{aligned} \tag{2.3}$$

and satisfy $\sqrt{v_1^2 + v_2^2} \equiv v \simeq 246$ GeV [1]. We parameterize the two Higgs doublets as

$$\Phi_i = \begin{pmatrix} \phi_i^+ \\ \frac{1}{\sqrt{2}}(v_i + R_i + iI_i) \end{pmatrix}, \qquad (i = 1, 2). \tag{2.4}$$

The Higgs mass matrices are diagonalized by performing the following rotation transformations:

$$\begin{pmatrix} H^0 \\ h^0 \end{pmatrix} = R(\alpha) \begin{pmatrix} R_1 \\ R_2 \end{pmatrix}, \quad \begin{pmatrix} G^0 \\ A^0 \end{pmatrix} = R(\beta) \begin{pmatrix} I_1 \\ I_2 \end{pmatrix}, \quad \begin{pmatrix} G^+ \\ H^+ \end{pmatrix} = R(\beta) \begin{pmatrix} \phi_1^+ \\ \phi_2^+ \end{pmatrix}, \tag{2.5}$$

where the rotation matrix R is defined as

$$R(\theta) = \begin{pmatrix} \cos\theta & \sin\theta \\ -\sin\theta & \cos\theta \end{pmatrix}, \tag{2.6}$$

α is the mixing angle between the two CP-even Higgs fields R_1 and R_2, and $\tan\beta = v_2/v_1$. The fields G^0 and $G^\pm$ are Nambu-Goldstone bosons and their three degrees of freedom are got "eaten" by the longitudinal components of Z and $W^\pm$ bosons, and induce the masses of weak gauge bosons. Therefore, the 2HDM predicts five scalar particles: h^0, H^0, A^0 and $H^\pm$. We may choose the following seven independent "physical" parameters as the inputs of the Higgs sector:

$$m_{h^0}, \quad m_{H^0}, \quad m_{A^0}, \quad m_{H^\pm}, \quad \sin\alpha, \quad \tan\beta, \quad v. \tag{2.7}$$

Then the quartic couplings $\lambda_{1,...,5}$ can be expressed in terms of these physical parameters as

$$\begin{aligned} &\lambda_1 = \frac{1}{v^2\cos^2\beta}\left(m_{h^0}^2\sin^2\alpha + m_{H^0}^2\cos^2\alpha\right), \quad \lambda_2 = \frac{1}{v^2\sin^2\beta}\left(m_{h^0}^2\cos^2\alpha + m_{H^0}^2\sin^2\alpha\right), \\ &\lambda_3 = 2\frac{m_{H^\pm}^2}{v^2} + \frac{\sin 2\alpha}{v^2\sin 2\beta}\left(m_{H^0}^2 - m_{h^0}^2\right), \quad \lambda_4 = \frac{1}{v^2}\left(m_{A^0}^2 - 2m_{H^\pm}^2\right), \quad \lambda_5 = -\frac{1}{v^2}m_{A^0}^2. \end{aligned} \tag{2.8}$$

[1] In this paper, the VEV v is fixed by the masses of weak gauge bosons M_W, M_Z and Fermi constant G_F.

	WW, ZZ	up-type quarks	down-type quarks, leptons
h^0	$\sin(\beta-\alpha)$	$\cos\alpha/\sin\beta$	$-\sin\alpha/\cos\beta$
H^0	$\cos(\beta-\alpha)$	$\sin\alpha/\sin\beta$	$\cos\alpha/\cos\beta$
A^0	0	$i\gamma^5\cot\beta$	$i\gamma^5\tan\beta$

Table 1: Tree-level couplings of the neutral Higgs bosons of the 2HDM(II) to gauge bosons and fermions. Each coupling is normalized to the corresponding coupling of the SM Higgs boson.

The tree-level couplings of h^0, H^0 and A^0 to the SM gauge bosons and fermions with respect to the corresponding couplings of the SM Higgs boson are presented in Table 1. It should be mentioned that the couplings of the CP-even Higgs bosons h^0 and H^0 have the same structures as those of the SM Higgs boson, while the Feynman rules for the $A^0 - f - \bar{f}$ interactions contain an additional factor $i\gamma^5$ since A^0 is a pseudoscalar. We can see from the table that when $(\beta-\alpha) \to \frac{\pi}{2}$, the couplings of the light CP-even Higgs h^0 to gauge bosons and fermions approach the corresponding SM ones, and the couplings of the heavy CP-even Higgs H^0 to weak gauge bosons approach zero. Therefore, the CP-even Higgs H^0 decouples from the VBF process $pp \to V^*V^* + 2\ jets \to h^0h^0 + 2\ jets$ in the SM limit of $(\beta-\alpha) = \frac{\pi}{2}$. In this work we use $\sin(\beta-\alpha)$ as an input parameter of the Higgs sector instead of $\sin\alpha$ to manifest the effects on the Higgs couplings to gauge bosons involved in the VBF h^0 pair production, considering the fact that the Higgs couplings to weak gauge bosons are proportional to $\sin(\beta-\alpha)$ and $\cos(\beta-\alpha)$.

3 Calculation Strategy

The SF approach is a very good approximation for studing the VBF processes at hadron colliders, which is accurate at a precision level well above the typical residual scale and parton distribution function (PDF) uncertainties [12]. This approximation is based on the absence or smallness of the QCD interference between the two inclusive final proton remnants. The Higgs boson pair production via VBF is a pure electroweak process at the LO, see Fig.1. There are two types of topological Feynman diagrams (t- and u-channel) contributing to the VBF Higgs pair production at parton level. The cross section is approximately contributed only by the squared t- and u-channel amplitudes, while their interference contribution is below 0.01%. Therefore, the VBF Higgs pair production can be viewed as the double deep-inelastic scattering (DIS) of two (anti)quarks with two virtual weak vector bosons independently emitted from the hadronic initial states fusing into a Higgs boson pair [8]. The

cross section can be calculated in terms of the charged-current and neutral-current hadronic structure functions $F_i^V(x,Q^2)$ $(i=1,2,3,\ V=Z,W^\pm)$ by adopting the SF approach [9]. This method has been implemented to calculate the NNLO QCD corrections to the single Higgs production via VBF [12,13]. Analogous to the case of the VBF single Higgs production, the nonfactorization contribution to the VBF Higgs pair production can also be safely neglected [13]. In this paper we adopt the SF approach to calculate the total inclusive cross section and differential distributions in the 2HDM(II) at the QCD NNLO for the VBF Higgs pair production $pp \to V^*V^* + 2\ jets \to h^0h^0 + 2\ jets$.

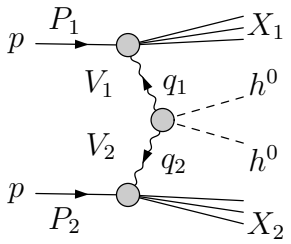

Figure 1: Light CP-even Higgs pair production via VBF.

The differential cross section for the VBF Higgs pair production can be expressed as [13]

$$\begin{aligned} d\sigma &= \sum_{(V_1V_2)} \frac{1}{2S} 2G_F^2 M_{V_1}^2 M_{V_2}^2 \frac{1}{\left(Q_1^2+M_{V_1}^2\right)^2} \frac{1}{\left(Q_2^2+M_{V_2}^2\right)^2} W_{\mu\nu}^{V_1}(x_1,Q_1^2)\mathcal{M}_{V_1V_2}^{\mu\rho}\mathcal{M}_{V_1V_2}^{*\nu\sigma} W_{\rho\sigma}^{V_2}(x_2,Q_2^2) \\ &\times \frac{d^3\vec{P}_{X_1}}{(2\pi)^3\,2E_{X_1}} \frac{d^3\vec{P}_{X_2}}{(2\pi)^3\,2E_{X_2}} ds_1 ds_2 dPS_2(k_1,k_2)\,(2\pi)^4\,\delta^4\left(P_1+P_2-P_{X_1}-P_{X_2}-\sum_{j=1,2}k_j\right), \end{aligned} \tag{3.1}$$

where $(V_1V_2)=(ZZ),(W^+W^-),(W^-W^+)$, G_F is the Fermi constant, $\sqrt{S}$ is the center-of-mass energy of the hadron collider, $dPS_2(k_1,k_2)$ represents the phase space of the final two Higgs bosons, $\mathcal{M}_{V_1V_2}^{\mu\nu}$ stands for the matrix element for the VBF subprocess $V_1(-q_1)+V_2(-q_2)\to h^0(k_1)+h^0(k_2)$, the physical scale Q is given by $Q_i^2=-q_i^2$ for $x=x_i$ $(i=1,2)$ and $x_i=Q_i^2/(2P_i\cdot q_i)$ are the usual DIS variables, and $s_i=(P_i+q_i)^2$ are the invariant mass of the i-th proton remnant. At the end of Eq.(3.1) there includes the four-body final state phase space element for the VBF Higgs pair production process, which is expressed explicitly in Appendix A.

The DIS hadronic tensor $W_{\mu\nu}^V(x,Q^2)$ can be expressed in terms of the standard DIS structure functions $F_j^V(x_i,Q_i^2)$ $(i=1,2,\ j=1,2,3)$ as

$$W_{\mu\nu}^V(x_i,Q_i^2)=\left(-g_{\mu\nu}+\frac{q_{i,\mu}q_{i,\nu}}{q_i^2}\right)F_1^V(x_i,Q_i^2)+\frac{\hat{P}_{i,\mu}\hat{P}_{i,\nu}}{P_i\cdot q_i}F_2^V(x_i,Q_i^2)+i\epsilon_{\mu\nu\alpha\beta}\frac{P_i^\alpha q_i^\beta}{2P_i\cdot q_i}F_3^V(x_i,Q_i^2),\quad (V=Z,W^\pm), \tag{3.2}$$

where $\epsilon_{\mu\nu\alpha\beta}$ is the completely antisymmetric tensor and the momentum $\hat{P}_i$ is defined as

$$\hat{P}_{i,\mu} = P_{i,\mu} - \frac{P_i \cdot q_i}{q_i^2} q_{i,\mu}. \tag{3.3}$$

Due to the CP conservation and the identity of the two final Higgs bosons, the matrix element for the $W^-(-q_1) + W^+(-q_2) \to h^0(k_1) + h^0(k_2)$ process is the same as that for the $W^+(-q_1) + W^-(-q_2) \to h^0(k_1) + h^0(k_2)$ process, i.e., $\mathcal{M}^{\mu\nu}_{W^-W^+} = \mathcal{M}^{\mu\nu}_{W^+W^-}$. Here we depict the Feynman diagrams for the $ZZ \to h^0h^0$ and $W^+W^- \to h^0h^0$ processes in Fig.2 and Fig.3, respectively, and the explicit expressions for $\mathcal{M}^{\mu\nu}$ are presented in Appendix B. Then the squared DIS hadronic tensor in Eq.(3.1) can be written in the form as

$$W^{V_1}_{\mu\nu}(x_1, Q_1^2)\mathcal{M}^{\mu\rho}_{V_1V_2}\mathcal{M}^{*\nu\sigma}_{V_1V_2}W^{V_2}_{\rho\sigma}(x_2, Q_2^2) = \sum_{i,j=1}^{3} C_{ij}^{V_1V_2} F_i^{V_1}(x_1, Q_1^2) F_j^{V_2}(x_2, Q_2^2), \tag{3.4}$$

where $C_{ij}^{V_1V_2}$ can be automatically generated by using the Mathematica packages FeynArts [19] and FeynCalc [20].

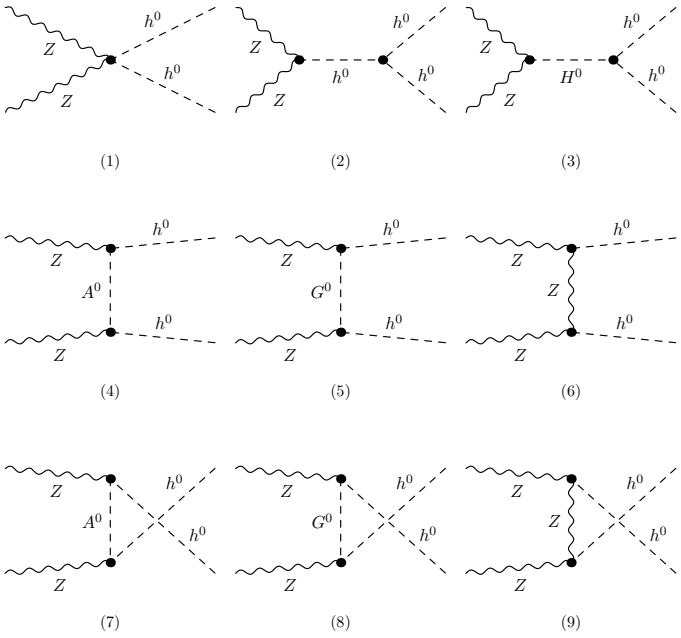

Figure 2: Feynman diagrams for the $ZZ \to h^0h^0$ process.

Within the QCD factorization formalism, the structure functions can be expressed as convolutions of the PDFs in proton with the short-distance Wilson coefficient functions. We denote the gluon, quark and antiquark PDFs at the factorization scale μ_f by $g(x, \mu_f)$, $q_i(x, \mu_f)$ and $\bar{q}_i(x, \mu_f)$, respectively,

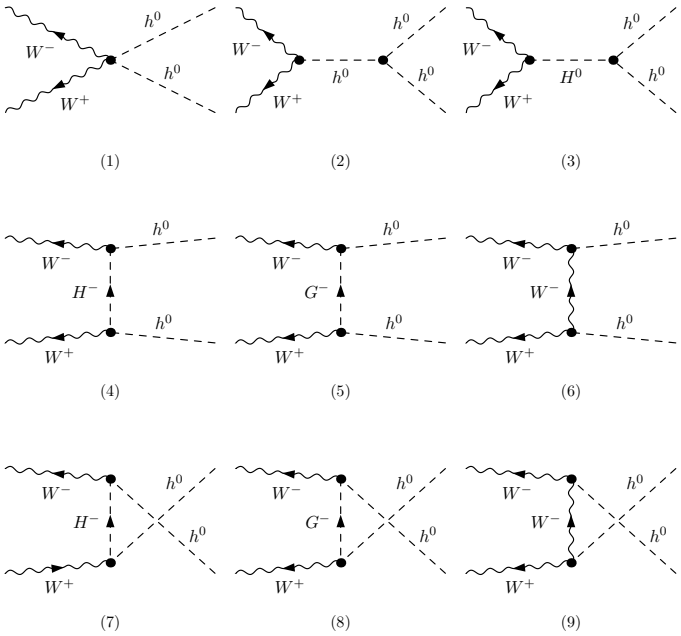

Figure 3: Feynman diagrams for the $W^+W^- \to h^0h^0$ process.

where the subscript i indicates the flavor of the (anti)quark. It is often convenient to write the DIS structure functions in terms of the gluon, and the following singlet and non-singlet quark distributions,

$$\begin{aligned} q_{\rm s} &= \sum_{i=1}^{n_f} \left(q_i + \bar{q}_i\right), && \text{(singlet)}, \\ q^{\rm v}_{\rm ns} &= \sum_{i=1}^{n_f} \left(q_i - \bar{q}_i\right), \quad q^{\pm}_{{\rm ns},ij} = \left(q_i \pm \bar{q}_i\right) - \left(q_j \pm \bar{q}_j\right), && \text{(non-singlets)}. \end{aligned} \tag{3.5}$$

For the Z-exchange neutral current, the DIS structure functions F_i^Z $(i = 1, 2, 3)$ can be written as follows [13]:

$$\begin{aligned} F_i^Z(x,Q^2) &= 2f_i(x) \int_0^1 dy \int_0^1 dz \delta(x - yz) \sum_{j=1}^{n_f} \left(v_j^2 + a_j^2\right) \\ &\quad \times \Big[q^+_{{\rm ns},j}(y,\mu_f) C^+_{i,{\rm ns}}(z,Q,\mu_r,\mu_f) + q_{\rm s}(y,\mu_f) C_{i,{\rm q}}(z,Q,\mu_r,\mu_f) + g(y,\mu_f) C_{i,{\rm g}}(z,Q,\mu_r,\mu_f) \Big], \\ F_3^Z(x,Q^2) &= 2f_3(x) \int_0^1 dy \int_0^1 dz \delta(x - yz) \sum_{j=1}^{n_f} 2v_j a_j \\ &\quad \times \Big[q^-_{{\rm ns},j}(y,\mu_f) C^-_{3,{\rm ns}}(z,Q,\mu_r,\mu_f) + q^{\rm v}_{\rm ns}(y,\mu_f) C^{\rm v}_{3,{\rm ns}}(z,Q,\mu_r,\mu_f) \Big], \end{aligned} \tag{3.6}$$

where $i = 1, 2$, $f_1(x) = 1/2$, $f_2(x) = x$, $f_3(x) = 1$, and the non-singlet quark densities $q^{\pm}_{{\rm ns},i}$ are obtained from $q^{\pm}_{{\rm ns},ij}$ as

$$q^{\pm}_{{\rm ns},i} = \sum_{j=1}^{n_f} q^{\pm}_{{\rm ns},ij} \ , \qquad (i = 1, ..., n_f). \tag{3.7}$$

The vector and axial-vector couplings of quark pair to Z boson used in Eqs.(3.6) are given by

$$v_i = I_i^3 - 2Q_i \sin^2\theta_W, \qquad a_i = I_i^3, \tag{3.8}$$

where Q_i and I_i^3 are the electric charge and weak isospin of the quark q_i, respectively.

For the W-exchange charged current, the DIS structure functions $F_i^{W^\mp}$ $(i = 1, 2, 3)$ are expressed as follows:

$$\begin{aligned}
F_i^{W^\mp}(x,Q^2) &= f_i(x)\int_0^1 dy\int_0^1 dz\delta(x-yz)\frac{1}{n_f}\sum_{j=1}^{n_f}\left(v_j^2+a_j^2\right) \\
&\quad\times\Big[\pm\delta q_{\rm ns}^-(y,\mu_f)C_{i,\rm ns}^-(z,Q,\mu_r,\mu_f)+q_{\rm s}(y,\mu_f)C_{i,\rm q}(z,Q,\mu_r,\mu_f)+g(y,\mu_f)C_{i,\rm g}(z,Q,\mu_r,\mu_f)\Big], \\
F_3^{W^\mp}(x,Q^2) &= f_3(x)\int_0^1 dy\int_0^1 dz\delta(x-yz)\frac{1}{n_f}\sum_{j=1}^{n_f}2v_ja_j \\
&\quad\times\Big[\pm\delta q_{\rm ns}^+(y,\mu_f)C_{3,\rm ns}^+(z,Q,\mu_r,\mu_f)+q_{\rm ns}^{\rm v}(y,\mu_f)C_{3,\rm ns}^{\rm v}(z,Q,\mu_r,\mu_f)\Big],
\end{aligned} \tag{3.9}$$

where the non-singlet quark densities $\delta q_{\rm ns}^\pm$ are defined in terms of $q_{{\rm ns},ij}^\pm$ as

$$\delta q_{\rm ns}^\pm = \sum_{i\in{\rm up},\ j\in{\rm down}} q_{{\rm ns},ij}^\pm\ , \tag{3.10}$$

and the vector and axial-vector couplings for charged current are given by

$$v_i = a_i = \frac{1}{\sqrt{2}}. \tag{3.11}$$

We can see from Eqs.(3.6) and Eqs.(3.9) that the renormalization and factorization scales for quark densities in each proton ($\mu_{1,r}$, $\mu_{2,r}$, $\mu_{1,f}$ and $\mu_{2,f}$) enter in Eq.(3.1). The Wilson coefficient functions in Eq.(3.6) and Eq.(3.9) parameterize the hard partonic scattering process and can be perturbatively expanded in powers of α_s. Up to the second order in α_s, $C_{3,\rm ns}^{\rm v} = C_{3,\rm ns}^-$, and the perturbative expansion of these Wilson coefficient functions reads

$$\begin{aligned}
C_{i,\rm ns}^\pm &= \delta(1-x)+a_s\left[c_{i,\rm ns}^{(1),\pm}+L_MP_{\rm ns}^{(0),\pm}\right] \\
&\quad+a_s^2\left[c_{i,\rm ns}^{(2),\pm}+L_M\left(P_{\rm ns}^{(1),\pm}+c_{i,\rm ns}^{(1),\pm}\otimes\left(P_{\rm ns}^{(0),\pm}-\beta_0\right)\right)+L_M^2\left(\frac{1}{2}P_{\rm ns}^{(0),\pm}\otimes\left(P_{\rm ns}^{(0),\pm}-\beta_0\right)\right)\right. \\
&\quad\left.+\beta_0L_R\left(c_{i,\rm ns}^{(1),\pm}+L_MP_{\rm ns}^{(0),\pm}\right)\right], \qquad\qquad (i=1,2,3),
\end{aligned} \tag{3.12}$$

$$C_{i,\rm q} = \delta(1-x)+a_s\left[c_{i,\rm q}^{(1)}+L_MP_{\rm qq}^{(0)}\right]$$

$$
\begin{aligned}
&+ a_s^2\Bigg[c_{i,\mathrm{q}}^{(2)} + L_M\left(P_{\mathrm{qq}}^{(1)} + c_{i,\mathrm{q}}^{(1)} \otimes (P_{\mathrm{qq}}^{(0)} - \beta_0) + c_{i,\mathrm{g}}^{(1)} \otimes P_{\mathrm{gq}}^{(0)}\right) \\
&+ L_M^2\left(\frac{1}{2}P_{\mathrm{qq}}^{(0)} \otimes (P_{\mathrm{qq}}^{(0)} - \beta_0) + \frac{1}{2}P_{\mathrm{qg}}^{(0)} \otimes P_{\mathrm{gq}}^{(0)}\right) \\
&+ \beta_0 L_R\left(c_{i,\mathrm{q}}^{(1)} + L_M P_{\mathrm{qq}}^{(0)}\right)\Bigg], \qquad (i = 1, 2),
\end{aligned} \tag{3.13}
$$

$$
\begin{aligned}
C_{i,\mathrm{g}} \;=\;& a_s\left[c_{i,\mathrm{g}}^{(1)} + L_M P_{\mathrm{qg}}^{(0)}\right] \\
&+ a_s^2\Bigg[c_{i,\mathrm{g}}^{(2)} + L_M\left(P_{\mathrm{qg}}^{(1)} + c_{i,\mathrm{q}}^{(1)} \otimes P_{\mathrm{qg}}^{(0)} + c_{i,\mathrm{g}}^{(1)} \otimes (P_{\mathrm{gg}}^{(0)} - \beta_0)\right) \\
&+ L_M^2\left(\frac{1}{2}P_{\mathrm{qq}}^{(0)} \otimes P_{\mathrm{qg}}^{(0)} + \frac{1}{2}P_{\mathrm{qg}}^{(0)} \otimes (P_{\mathrm{gg}}^{(0)} - \beta_0)\right) \\
&+ \beta_0 L_R\left(c_{i,\mathrm{g}}^{(1)} + L_M P_{\mathrm{qg}}^{(0)}\right)\Bigg], \qquad (i = 1, 2),
\end{aligned} \tag{3.14}
$$

where $a_s = \alpha_s(\mu_r)/(4\pi)$, $L_M = \ln(Q^2/\mu_f^2)$, $L_R = \ln(\mu_r^2/\mu_f^2)$, $\beta_0 = (11C_A - 2n_f)/3$ is referred to the one-loop beta-function coefficient, and $\otimes$ represents the standard Mellin convolution. It should be noted that [2]

$$
P_{\mathrm{ns}}^{(0),\pm} = P_{\mathrm{qq}}^{(0)}, \qquad\qquad c_{i,\mathrm{ns}}^{(1),\pm} = c_{i,\mathrm{q}}^{(1)}, \quad (i = 1, 2, 3). \tag{3.15}
$$

The two-loop order quark-quark splitting function $P_{\mathrm{qq}}^{(1)}$ and the quark singlet DIS coefficient functions $c_{i,\mathrm{q}}^{(2)}$ are usually expressed as

$$
P_{\mathrm{qq}}^{(1)} = P_{\mathrm{ns}}^{(1),+} + P_{\mathrm{ps}}^{(1)}, \qquad\qquad c_{i,\mathrm{q}}^{(2)} = c_{i,\mathrm{ns}}^{(2),+} + c_{i,\mathrm{ps}}^{(2)}, \quad (i = 1, 2), \tag{3.16}
$$

where $P_{\mathrm{ps}}^{(1)}$ and $c_{i,\mathrm{ps}}^{(2)}$ are the pure-singlet contributions at the second order of α_s. All the DIS coefficient functions $c_{i,\mathrm{q}}^{(1)}$, $c_{3,\mathrm{q}}^{(1)}$, $c_{i,\mathrm{g}}^{(1)}$, $c_{i,\mathrm{ns}}^{(2),\pm}$, $c_{i,\mathrm{ps}}^{(2)}$, $c_{i,\mathrm{g}}^{(2)}$ $(i = 1, 2)$ and the splitting functions $P_{\mathrm{qq}}^{(0)}$, $P_{\mathrm{qg}}^{(0)}$, $P_{\mathrm{gq}}^{(0)}$, $P_{\mathrm{gg}}^{(0)}$, $P_{\mathrm{ns}}^{(1),\pm}$, $P_{\mathrm{ps}}^{(1)}$, $P_{\mathrm{qg}}^{(1)}$ used in Eqs.(3.12)-(3.14) are given in Refs. [21–25]. They can be easily evaluated in terms of harmonic polylogarithms $H_{\vec{m}}(x)/(1 \pm x)$ [26]. In this paper we adopt the FORTRAN program Hplog [27] to implement numerical calculation of harmonic polylogarithms.

4 Numerical results and discussion

In this section we present the integrated cross sections and some kinematic distributions for the light CP-even Higgs pair production via VBF at $\sqrt{S} = 14$, 33 and 100 TeV proton-proton colliders up to

[2] For $i = 3$, the coefficient functions $c_{3,\mathrm{ns}}^{(1),\pm}(x)$ satisfy $c_{3,\mathrm{ns}}^{(1),+}(x) = c_{3,\mathrm{ns}}^{(1),-}(x)$ and are defined as $c_{3,\mathrm{q}}^{(1)}(x)$.

	$\sin(\beta-\alpha)$	$\tan\beta$	m_{h^0} (GeV)	m_{H^0} (GeV)	m_{A^0} (GeV)	$m_{H^\pm}$ (GeV)
B1	0.6	2	126	275	600	600
B2	1	1.5	126	160	380	420

Table 2: The 2HDM benchmark points.

the QCD NNLO by employing the SF approach. In our numerical calculations we use the following values for the electroweak parameters:

$$M_W = 80.385 \text{ GeV}, \qquad M_Z = 91.1876 \text{ GeV}, \qquad G_F = 1.1663787 \times 10^{-5} \text{ GeV}^{-2}. \tag{4.1}$$

The Weinberg angle is fixed in the on-shell scheme as $\sin^2\theta_W = 1 - M_W^2/M_Z^2$. We choose the 2HDM(II) input parameters at two benchmark points, B1 and B2, for demonstration and comparison, whose related parameters are listed in Table 2. The parameters at both the B1 and B2 points survive in the present theoretical and experimental constraints [17]. At the benchmark point B1 we have $m_{H^0} > 2m_{h^0}$ and there exists H^0 resonance effect in the VBF h^0-pair production process. While at the benchmark point B2 there does not exist H^0 resonance effect, and the corresponding results should be the same with those in the SM case for the VBF $h^0h^0 + 2\ jets$ production process. The width of H^0 can be calculated by using 2HDMC program [18], and at the benchmark point B1 we get the total decay width of H^0 boson being $\Gamma_{H^0} = 5.484$ GeV.

We adopt the MSTW2008 PDFs [28] in the convolutions of parton densities with Wilson coefficient functions. In the calculations of the ZZ-fusion contributions (see Fig.2), we take the b-quark as a massless parton and the number of massless flavors $n_f = 5$ in Eqs.(3.6). While in the evaluations of the WW-fusion process (see Fig.3), the initial b-quark is not included since it would produce a top-quark in the final state. In the following analysis we take $\mu = \mu_f = \mu_r$ for simplicity and the typical central value of the renormalization/factorization scale is fixed by the corresponding vector-boson momentum transfer $\mu^2 = -q_i^2 = Q^2$ for $i = 1, 2$ [3], if there is no other statement. Furthermore, we put a lower bound of $Q^2 > 4$ GeV^2 in order to keep in the perturbative regime, and the independence of the integrated cross section on this technical Q cut has been checked numerically.

[3]Here the scale $\mu^2 = Q^2$ means $\mu_1^2 = \mu_{1,f}^2 = \mu_{1,r}^2 = Q_1^2$ and $\mu_2^2 = \mu_{2,f}^2 = \mu_{2,r}^2 = Q_2^2$.

4.1 Dependence on 2HDM(II) parameters

The integrated cross section for the VBF light, neutral CP-even Higgs boson pair production is related to the 2HDM(II) parameters, such as the two CP-even Higgs boson masses, ratio of the VEVs and the mixing angle between the two CP-even Higgs bosons. In this subsection we study the dependence of integrated cross section for the VBF $h^0h^0 + 2\ jets$ production on the related model parameters at the $\sqrt{S} = 14$ TeV LHC by adopting above event selection scheme.

In Fig.4(a) we depict the LO and NNLO QCD corrected integrated cross sections as functions of m_{H^0} with the other related model parameters being the values at the benchmark point B1. We see from the figure that there is a steep increment at the position of $m_{H^0} \sim 2m_{h^0} = 252$ GeV due to the on-shell H^0 decay of $H^0 \to h^0h^0$, and H^0 resonance effect enhances the production rate obviously in the region of $m_{H^0} > 260$ GeV. It shows also that the QCD corrections up to NNLO always increase the LO cross section particularly for the large H^0 mass.

Fig.4(b) shows the dependence of the LO and QCD NNLO corrected integrated cross sections on the ratio of the VEVs $\tan\beta$. There we fix all the 2HDM(II) parameters are the values of the benchmark point B1 except $\tan\beta$, which varies from 0.5 to 10. The figure demonstrates that both the LO and NNLO corrected total cross sections reach their minimal and maximal values at the positions about $\tan\beta \sim 0.75$ and 6.0, respectively. In the region of $\tan\beta > 4.0$, both the LO and the NNLO QCD corrected cross sections exceed 600 fb.

We plot Fig.4(c) to show the dependence of the LO and NNLO QCD corrected integrated cross sections on the parameter $\sin(\beta - \alpha)$ with the other related 2HDM(II) parameters being fixed at the benchmark point B1, i.e., $\tan\beta = 2$ and $m_{H^0} = 275$ GeV. It shows obviously that both the LO and the NNLO QCD corrected total cross sections reach their maxima at the position of $\sin(\beta - \alpha) = 0.2$, and then decrease with the increment of $\sin(\beta - \alpha)$ from 0.2 to 0.9.

4.2 Theoretical uncertainties of integrated cross section

In order to make a precision comparison between the theoretical predictions and experimental measurements, we should assess thoroughly the theoretical uncertainties affecting the central predictions of the total cross sections. For some production processes at hadron colliders, such as $pp \to V^*V^* \to h^0h^0 + 2\ jets$ process, the theoretical uncertainty mainly comes from the missing higher order correc-

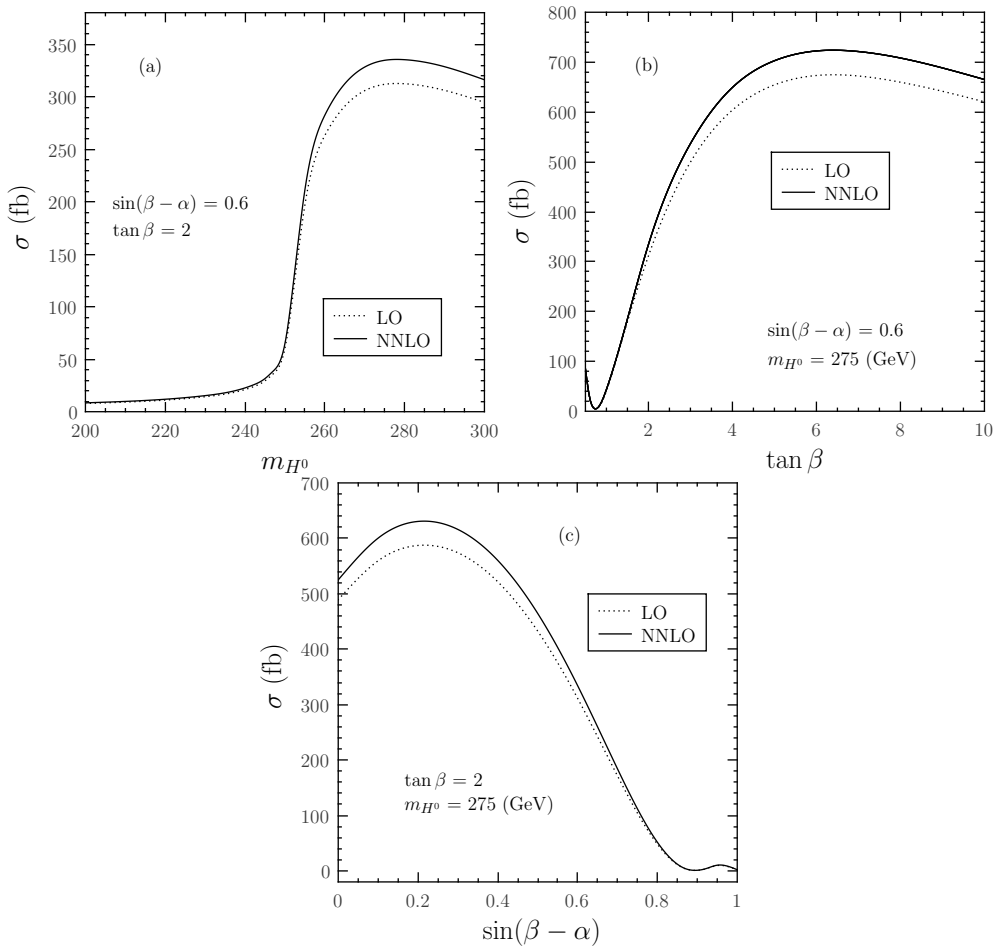

Figure 4: The dependence of the LO and NNLO QCD corrected integrated cross sections for the VBF $h^0h^0+2\ jets$ production on the 2HDM(II) parameters at the $\sqrt{S}=14$ TeV LHC. (a) as the function of the H^0 boson mass, (b) as the function of the $\tan\beta$, (c) as the function of the parameter $\sin(\beta-\alpha)$.

tions, PDFs and α_s.

4.2.1 Scale uncertainty

The uncertainty due to missing higher order radiative corrections can be estimated by varying the factorization/renormalization scale μ around a central value that is taken close to the physical scale of the process. A conventional range of variation for the VBF process is

$$\frac{1}{4}Q \leq \mu \leq 4Q, \tag{4.2}$$

where the central value Q of μ_r and μ_f is the virtuality of the vector bosons which fuse into the Higgs boson pair. In Figs.5(a) and (b) we present the scale dependence of the LO, QCD NLO and NNLO corrected integrated cross sections for the VBF $h^0h^0+2\ jets$ production at the $\sqrt{S}=14$ TeV

	σ_{LO} (fb)	σ_{NLO} (fb)	σ_{NNLO} (fb)
B1	$311.30^{+32.38\ (+10\%)}_{-28.88\ (-9\%)}$	$333.20^{+2.51\ (+0.8\%)}_{-12.08\ (-3.6\%)}$	$334.18^{+9.82\ (+2.9\%)}_{-1.83\ (-0.5\%)}$
B2	$1.858^{+0.374\ (+20\%)}_{-0.270\ (-15\%)}$	$1.976^{+0.00\ (+0.0\%)}_{-0.078\ (-3.9\%)}$	$1.986^{+0.045\ (+2.3\%)}_{-0.00\ (-0.0\%)}$

Table 3: The LO, QCD NLO and NNLO corrected integrated cross sections for the VBF $h^0h^0 + 2\ jets$ production at $\sqrt{S} = 14$ TeV LHC at the benchmark points B1 and B2. The scale uncertainties are obtained from the variation in the range of $\mu \in [Q/4,\ 4Q]$. The data in brackets are the relative uncertainties.

LHC at the benchmark points B1 and B2, respectively. The central values of the integrated cross sections and the corresponding errors due to missing higher order radiative corrections are listed in Table 3. From Figs.5(a, b) and Table 3 we find that the scale uncertainties of integrated cross sections can be significantly reduced by including higher order radiative corrections. For the benchmark B1 (B2), the corresponding relative upper and lower scale relative uncertainties, defined as: the upper limit of scale uncertainty $\equiv \frac{max[\sigma(\mu)-\sigma(\mu=Q)]}{\sigma(\mu=Q)}$, and the lower limit of scale uncertainty $\equiv \frac{min[\sigma(\mu)-\sigma(\mu=Q)]}{\sigma(\mu=Q)}$ with $\mu \in [Q/4,\ 4Q]$, are about $^{(+10\%)}_{(-9\%)}$ $\left(^{(+20\%)}_{(-15\%)}\right)$ at the LO, and are reduced to $^{(+0.8\%)}_{(-3.6\%)}$ $\left(^{(+0.0\%)}_{(-3.9\%)}\right)$ and $^{(+2.9\%)}_{(-0.5\%)}$ $\left(^{(+2.3\%)}_{(-0.0\%)}\right)$ at the QCD NLO and NNLO, respectively. We see that the variation of scale uncertainty of σ_{NNLO} is smaller than the corresponding ones of σ_{LO} and σ_{NLO}. Therefore, from the point of view of improving the scale uncertainty, the NNLO QCD corrections should be taken into account for the precision measurement of the VBF Higgs pair production process.

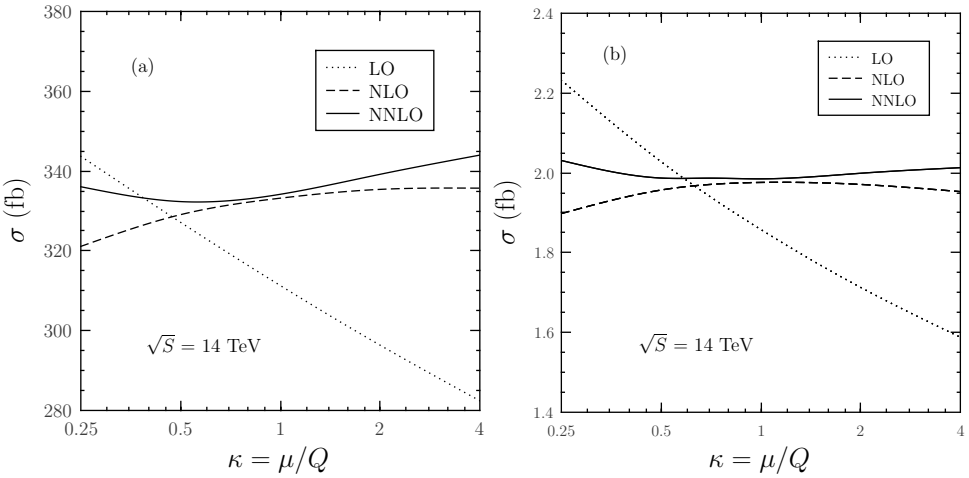

Figure 5: The scale dependence of the LO, QCD NLO and NNLO corrected integrated cross sections for the VBF $h^0h^0 + 2\ jets$ production at the $\sqrt{S} = 14$ TeV LHC. (a) at the benchmark point B1. (b) at the benchmark point B2.

Figs.5(a) and (b) also demonstrate that the impact of the NNLO QCD corrections at the central

scale Q is smaller than 1%. Compared with other values in the range $[Q/4, 4Q]$, the scale choice $\mu = Q$ is more natural because it exhibits a better convergence of the perturbative expansion. Therefore, we set the factorization/renormalization scale μ as its central value Q in the following numerical calculations.

4.2.2 PDF+α_s uncertainty

For a given parametrization of the PDFs such as MSTW2008, the PDF uncertainty comes from the experimental uncertainties on the fitted data. For a fixed value of α_s, MSTW2008 provides a central PDF set S_0 and $2n$ eigenvector PDF sets $S_i^{\pm}$ $(i = 1, ..., n,\ n = 20)$. The PDF uncertainties on the hadronic cross section are given by [29]

$$\begin{aligned}
\left(\Delta\sigma^{\alpha_s}_{PDF}\right)_+ &= \sqrt{\sum_{i=1}^{n}\left\{\max\left[\sigma^{\alpha_s}(S_i^+) - \sigma^{\alpha_s}(S_0),\ \sigma^{\alpha_s}(S_i^-) - \sigma^{\alpha_s}(S_0),\ 0\right]\right\}^2}, \\
\left(\Delta\sigma^{\alpha_s}_{PDF}\right)_- &= \sqrt{\sum_{i=1}^{n}\left\{\max\left[\sigma^{\alpha_s}(S_0) - \sigma^{\alpha_s}(S_i^+),\ \sigma^{\alpha_s}(S_0) - \sigma^{\alpha_s}(S_i^-),\ 0\right]\right\}^2},
\end{aligned} \tag{4.3}$$

where $\sigma^{\alpha_s}(S_0)$, $\sigma^{\alpha_s}(S_i^+)$ and $\sigma^{\alpha_s}(S_i^-)$ represent the cross sections obtained by using the PDF sets S_0, S_i^+ and S_i^-, respectively.

In additional to the PDF uncertainty, there is also an uncertainty due to the errors on the value of the strong coupling constant α_s. Beside the best-fit sets of PDFs which correspond to α_s^0, four more PDF sets corresponding to $\alpha_s = \alpha_s^0 \pm 0.5\sigma$ and $\alpha_s = \alpha_s^0 \pm 1\sigma$ are provided by the MSTW collaboration, where α_s^0 and σ are the central value and the standard deviation of α_s, respectively. Comparing the results obtained from the five sets, the pure α_s uncertainties are defined as

$$\begin{aligned}
(\Delta\sigma_{\alpha_s})_+ &= \max_{\alpha_s}\left[\sigma^{\alpha_s}(S_0)\right] - \sigma^{\alpha_s^0}(S_0), \\
(\Delta\sigma_{\alpha_s})_- &= \sigma^{\alpha_s^0}(S_0) - \min_{\alpha_s}\left[\sigma^{\alpha_s}(S_0)\right],
\end{aligned} \tag{4.4}$$

where max and min run over the five values of α_s.

For the MSTW2008 PDFs, the combined PDF+α_s uncertainties are given by [29]

$$\begin{aligned}
(\Delta\sigma_{PDF+\alpha_s})_+ &= \max_{\alpha_s}\left[\sigma^{\alpha_s}(S_0) + \left(\Delta\sigma^{\alpha_s}_{PDF}\right)_+\right] - \sigma^{\alpha_s^0}(S_0), \\
(\Delta\sigma_{PDF+\alpha_s})_- &= \sigma^{\alpha_s^0}(S_0) - \min_{\alpha_s}\left[\sigma^{\alpha_s}(S_0) - \left(\Delta\sigma^{\alpha_s}_{PDF}\right)_-\right].
\end{aligned} \tag{4.5}$$

$\sqrt{S}$ (TeV)		σ_{LO} (fb)	σ_{NLO} (fb)	σ_{NNLO} (fb)
14	B1	$311.30^{+32.38+4.06}_{-28.88-4.04}\left(^{+10.4\%+1.3\%}_{-9.3\%-1.3\%}\right)$	$333.20^{+2.51+8.46}_{-12.08-6.57}\left(^{+0.8\%+2.5\%}_{-3.6\%-2.0\%}\right)$	$334.18^{+9.82+7.36}_{-1.83-5.87}\left(^{+2.9\%+2.2\%}_{-0.5\%-1.8\%}\right)$
	B2	$1.858^{+0.374+0.028}_{-0.270-0.026}\left(^{+20.1\%+1.5\%}_{-14.5\%-1.4\%}\right)$	$1.976^{+0+0.052}_{-0.078-0.039}\left(^{+0\%+2.6\%}_{-3.9\%-2.0\%}\right)$	$1.986^{+0.045+0.048}_{-0-0.035}\left(^{+2.3\%+2.4\%}_{-0.0\%-1.8\%}\right)$
33	B1	$1404^{+0+15}_{-30-16}\left(^{+0\%+1.1\%}_{-2.1\%-1.1\%}\right)$	$1500^{+54+35}_{-74-32}\left(^{+3.6\%+2.3\%}_{-4.9\%-2.1\%}\right)$	$1503^{+73+32}_{-17-28}\left(^{+4.9\%+2.1\%}_{-1.1\%-1.9\%}\right)$
	B2	$11.234^{+0.878+0.129}_{-0.830-0.149}\left(^{+7.8\%+1.1\%}_{-7.4\%-1.3\%}\right)$	$12.002^{+0.190+0.297}_{-0.562-0.225}\left(^{+1.6\%+2.5\%}_{-4.7\%-1.9\%}\right)$	$12.041^{+0.359+0.258}_{-0.060-0.209}\left(^{+3.0\%+2.1\%}_{-0.5\%-1.7\%}\right)$
100	B1	$7271^{+770+73}_{-1130-81}\left(^{+10.6\%+1.0\%}_{-15.5\%-1.1\%}\right)$	$7554^{+535+188}_{-580-119}\left(^{+7.1\%+2.5\%}_{-7.7\%-1.6\%}\right)$	$7578^{+553+150}_{-134-170}\left(^{+7.3\%+2.0\%}_{-1.8\%-2.2\%}\right)$
	B2	$75.36^{+4.91+2.07}_{-6.34-1.07}\left(^{+6.5\%+2.7\%}_{-8.4\%-1.4\%}\right)$	$79.82^{+3.92+2.99}_{-5.26-1.95}\left(^{+4.9\%+3.7\%}_{-6.6\%-2.4\%}\right)$	$80.05^{+3.92+1.58}_{-0.80-1.48}\left(^{+4.9\%+2.0\%}_{-1.0\%-1.8\%}\right)$

Table 4: The LO, QCD NLO and NNLO corrected integrated cross sections for VBF $h^0h^0 + 2\ jets$ production at $\sqrt{S} = 14$, 33 and 100 TeV pp colliders at the benchmark points B1 and B2 together with scale uncertainties (the first ones) and combined 68% CL PDF+α_s uncertainties (the second ones). The data in brackets are the relative uncertainties.

If the dependence of $\left(\Delta\sigma^{\alpha_s}_{PDF}\right)_{\pm}$ on α_s is negligible, the overall PDF+α_s uncertainties can be approximately expressed as

$$(\Delta\sigma_{PDF+\alpha_s})_{\pm} \simeq (\Delta\sigma_{PDF})_{\pm} + (\Delta\sigma_{\alpha_s})_{\pm}\,, \tag{4.6}$$

where $(\Delta\sigma_{PDF})_{\pm} = (\Delta\sigma^{\alpha_s^0}_{PDF})_{\pm}$ are pure PDF uncertainties. In the following calculations, we adopt Eq.(4.6) to evaluate the combined PDF+α_s uncertainty.

4.2.3 Integrated cross sections

In Table 4 we present the LO, QCD NLO and NNLO corrected integrated cross sections for the VBF $h^0h^0+2\ jets$ production at $\sqrt{S} = 14$, 33 and 100 TeV pp hadron colliders at the benchmark points B1 and B2. The scale and combined PDF+α_s uncertainties are also provided to estimate the precisions of these perturbative predictions. From this table we can see that the factorization/renormalization scale and the combined PDF+α_s uncertainties are generally comparable, and both of them are reduced by NLO, NNLO QCD corrections. For both benchmarks of B1 and B2, the theoretical upper and lower deviations of the NNLO prediction at the 14 TeV LHC, which are obtained by adding linearly the scale and $PDF+\alpha_s$ uncertainties, are always bellow 5.1%. As the increment of pp colliding energy $\sqrt{S}$ from 14 TeV to 100 TeV, the NNLO QCD corrections increase the integrated cross sections and the combined uncertainties for the VBF Higgs pair production at the benchmarks B1 and B2 separately.

4.3 Kinematic distributions

Analogous to the VBF $h^0+2\,jets$ production, the signal of VBF $h^0h^0+2\,jets$ production involves two energetic forward and backward jets in association with two centrally produced Higgs bosons. This character plays an important role in discriminating the VBF signal from the heavy QCD background. Since a precision study of the kinematic distributions of the final Higgs bosons for the signal process is helpful in theoretical and experimental analyses, we provide the NNLO QCD corrected transverse momentum p_T, rapidity y and invariant mass M distributions of the final Higgs bosons for the VBF $h^0h^0+2\,jets$ production at pp colliders. In order to assess the impact of the NNLO QCD corrections, we introduce the differential NNLO QCD K-factor, which is defined as

$$K(x) = \frac{d\sigma_{NNLO}}{dx} \Big/ \frac{d\sigma_{LO}}{dx}, \tag{4.7}$$

where x stands for a kinematic variable.

The LO and NNLO QCD corrected transverse momentum distributions of the leading Higgs boson h_1^0 and the second Higgs boson h_2^0 at $\sqrt{S} = 14$, 33 and 100 TeV pp colliders at benchmark point B1 are shown in Figs.6(a1, a2, a3) and (b1, b2, b3), respectively, where the leading Higgs boson h_1^0 and the second Higgs boson h_2^0 are defined as

$$p_{Th_1^0} > p_{Th_2^0}\ . \tag{4.8}$$

We see from these figures that the NNLO QCD corrections can enhance the Higgs p_T distributions, but the K-factors are less than 1.10 for both $p_{Th_1^0}$ and $p_{Th_2^0}$ distributions in the plotted p_T range. The $p_{Th_1^0}$ distributions reach their maxima at $p_{Th_1^0} \sim 80$ GeV, while the $p_{Th_2^0}$ distributions reach their maxima at $p_{Th_2^0} \sim 45$ GeV, at $\sqrt{S} = 14,\ 33,\ 100$ TeV pp colliders, respectively.

The LO and NNLO QCD corrected rapidity distributions of the leading Higgs h_1^0 and the second Higgs h_2^0 at $\sqrt{S} = 14$, 33 and 100 TeV pp colliders at benchmark point B1 are plotted in Figs.7(a1, a2, a3) and (b1, b2, b3), respectively. From these figures we can see that the two final Higgs bosons prefer to be produced in the central rapidity region.

The LO and NNLO QCD corrected distributions of the invariant mass of final Higgs boson pair, $\frac{d\sigma_{(NN)LO}}{dM_{h^0h^0}}$, at the $\sqrt{S} = 14$ TeV LHC at benchmark points B1 and B2 are given in Figs.8(a) and (b), respectively. For benchmark B2, the Higgs pair invariant mass distributions are mostly concentrated

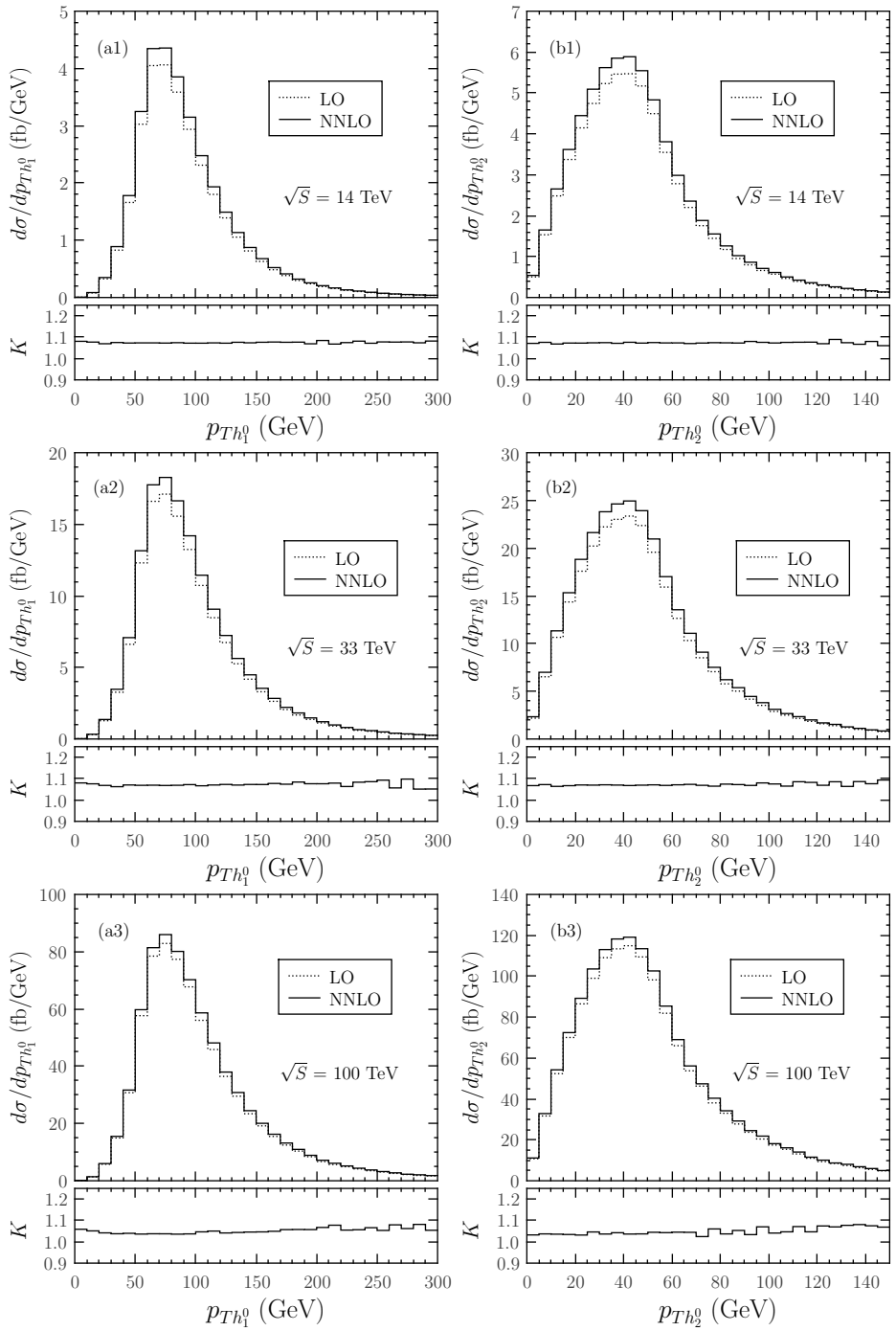

Figure 6: The LO, NNLO QCD corrected Higgs transverse momentum distributions and corresponding K-factors for the VBF h^0h^0+2 *jets* production at $\sqrt{S} = 14$, 33 and 100 TeV pp colliders at benchmark point B1. (a1), (a2) and (a3) are for the leading Higgs boson. (b1), (b2) and (b3) are for the second Higgs boson.

in the vicinity of $M_{h^0h^0} \sim 370$ GeV, and then decrease slowly with the increment of $M_{h^0h^0}$. The corresponding K-factors are in the range of [1.05, 1.09]. For benchmark B1, the $M_{h^0h^0}$ distributions

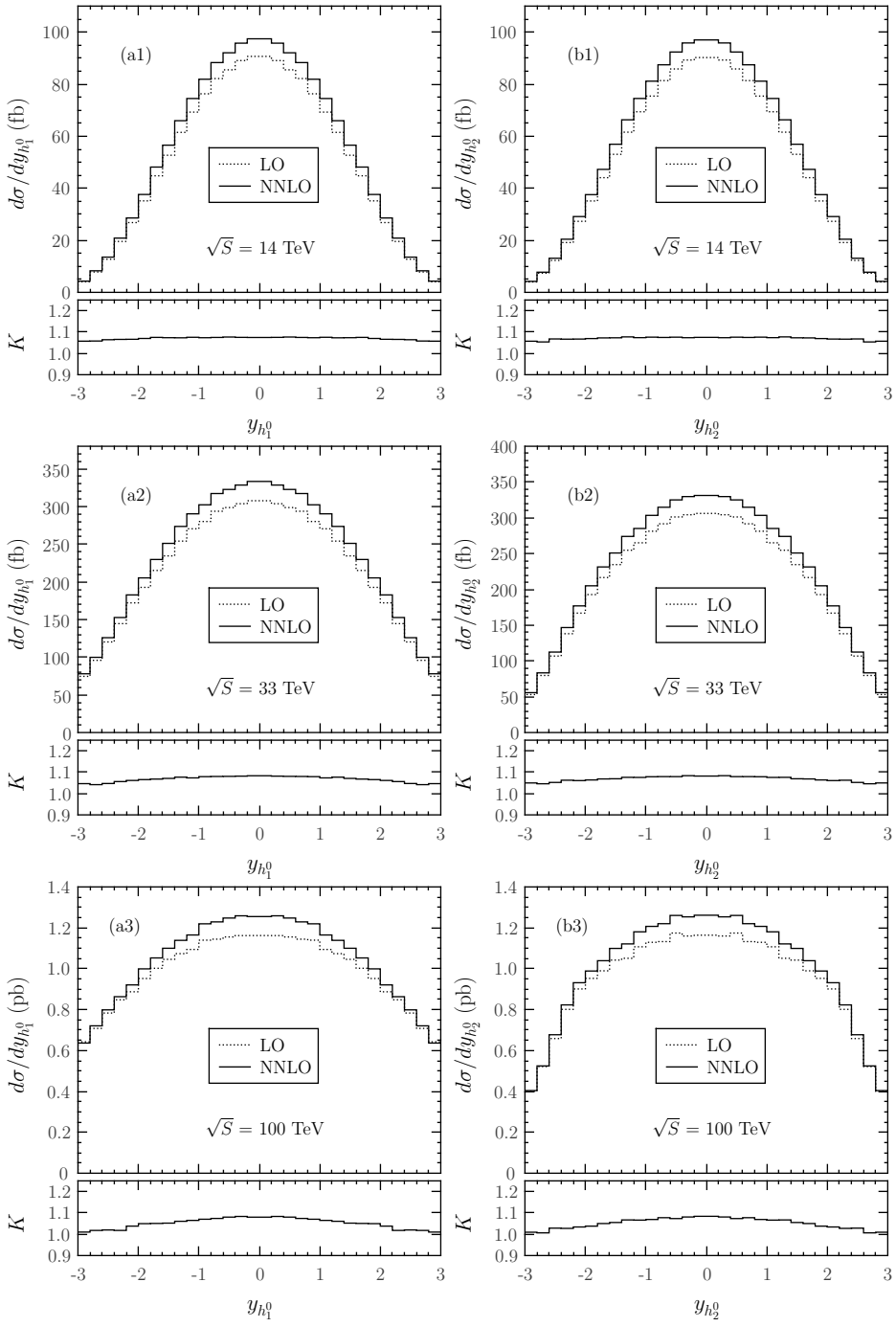

Figure 7: The LO, NNLO QCD corrected Higgs rapidity distributions and corresponding K-factors for VBF $h^0h^0 + 2\ jets$ production at $\sqrt{S} = 14$, 33 and 100 TeV pp colliders at benchmark point B1. (a1), (a2) and (a3) are for the leading Higgs boson. (b1), (b2) and (b3) are for the second Higgs boson.

are sharply enhanced at $M_{h^0h^0} \sim 276$ GeV due to the H^0 resonance effect. The total cross section for the VBF $h^0h^0 + 2\ jets$ production is dominated by the VBF $H^0 + 2\ jets$ production mechanism

with subsequent decay of $H^0 \to h^0 h^0$. By analyzing the invariant mass distribution of h^0-pair, we can directly probe the $\lambda_{h^0h^0h^0}$ and $\lambda_{H^0h^0h^0}$ trilinear Higgs self-couplings which can reconstruct the Higgs potential, and extract the resonance H^0 production signal.

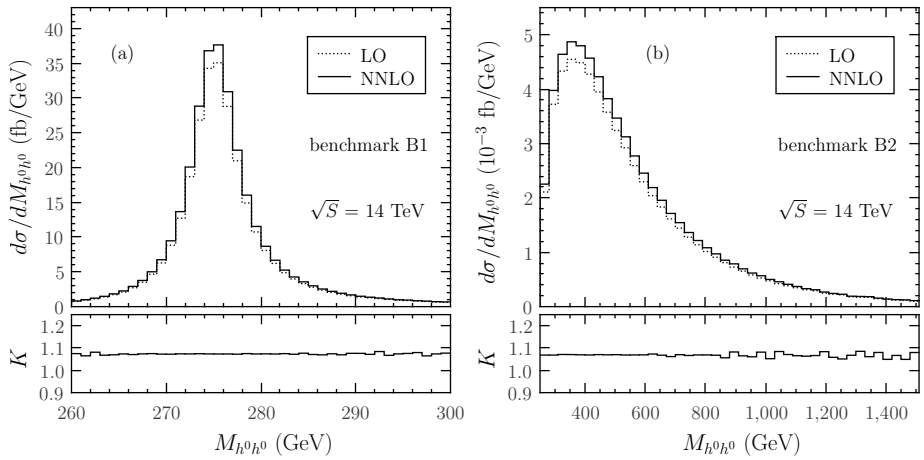

Figure 8: The LO, NNLO QCD corrected Higgs pair invariant mass distributions and corresponding K-factors for the VBF $h^0h^0 + 2\ jets$ production at 14 TeV LHC. (a) at the benchmark point B1. (b) at the benchmark point B2.

5 Summary

In this paper, we investigated in detail the light, CP-even Higgs pair production via VBF at pp colliders within the type-II 2HDM up to the QCD NNLO by adopting the structure function approach. We studied the dependence of the integrated cross section on the model parameters. To assess the theoretical uncertainty on the perturbative predictions, we considered both the factorization/renormalization scale uncertainty and the combined PDF+α_s uncertainty. Our numerical results show that the scale uncertainty is comparable with the combined PDF+α_s uncertainty, and can be reduced significantly by the QCD NNLO corrections. At the $\sqrt{S} = 14$ TeV LHC the total QCD NNLO corrected theoretical upper and lower deviations, defined as the linear combination of the scale and combined PDF+α_s uncertainties, are below 5.1%. We study also the kinematic distributions of the final Higgs bosons at the QCD NNLO by using the structure function approach, and obtain the phase space dependent K-factor. By analyzing $M_{h^0h^0}$ distribution, we could obtain the strength of the $\lambda_{H^0h^0h^0}$ coupling relative to the $\lambda_{h^0h^0h^0}$ coupling qualitatively, and extract the resonance H^0 production signal which provides a means of probing the extended Higgs sector.

Acknowledgments: This work was supported in part by the National Natural Science Foundation of China (Grants. No.11275190, No.11375008, No.11375171), and the Fundamental Research Funds for the Central Universities (Grant. No.WK2030040044).

Appendix

A Phase space element for VBF Higgs pair production process

Here we briefly document the parameterization for the phase space of the VBF Higgs pair production process. As shown in Fig.1, We denote the momenta of the incoming protons and outgoing proton remnants as P_i and P_{X_i} $(i = 1, 2)$, respectively. The Lorentz invariant four-body final state phase space element for the VBF Higgs pair production process (shown in Eq.(3.1)) can be rewritten as

$$dPS = \left[\prod_{i=1,2} ds_i \frac{d^4 P_{X_i}}{(2\pi)^4} 2\pi\delta\left(P_{X_i}^2 - s_i\right)\right] dPS_2(k_1, k_2)\,(2\pi)^4\,\delta^4\left(P_1 + P_2 - P_{X_1} - P_{X_2} - \sum_{j=1,2} k_j\right), \quad \text{(A.1)}$$

where k_1 and k_2 are the momenta of the two outgoing Higgs bosons, and

$$dPS_2(k_1, k_2) = \frac{d^3\vec{k}_1}{(2\pi)^3\,2E_1}\frac{d^3\vec{k}_2}{(2\pi)^3\,2E_2}. \quad \text{(A.2)}$$

By integrating out the invariant masses of proton remnants s_1 and s_2, and replacing the integral variables P_{X_i} with $q_i = P_{X_i} - P_i$, we obtain

$$dPS = \left[\prod_{i=1,2} \frac{d^4 q_i}{(2\pi)^3}\right] dPS_2(k_1, k_2)\,(2\pi)^4\,\delta^4\left(q_1 + q_2 + \sum_{j=1,2} k_j\right). \quad \text{(A.3)}$$

The integration measures can be expressed as

$$d^4 q_1 = \frac{Q_1^2}{x_1} dx_1 \frac{d^3\vec{k}_3}{2E_3}, \qquad d^4 q_2 = \frac{Q_2^2}{x_2} dx_2 \frac{d^3\vec{k}_4}{2E_4}, \quad \text{(A.4)}$$

where the light-like momenta k_3 and k_4 are defined as

$$k_3 = q_1 + x_1 P_1, \qquad k_4 = q_2 + x_2 P_2. \quad \text{(A.5)}$$

At the end we can express the phase space element in terms of the DIS variables x_i $(i = 1, 2)$ and the three-momenta of final Higgs bosons and the $\vec{k}_3$ and $\vec{k}_4$ as

$$dPS = \frac{Q_1^2 Q_2^2}{x_1 x_2} dx_1 dx_2 \left[\prod_{i=1}^{4} \frac{d^3\vec{k}_i}{(2\pi)^3\,2E_i}\right] (2\pi)^4\,\delta^4\left(x_1 P_1 + x_2 P_2 - \sum_{i=1}^{4} k_i\right). \quad \text{(A.6)}$$

B Matrix element $\mathcal{M}^{\mu\nu}$ for $VV \to h^0h^0$ subprocess

The matrix element for the $Z(-q_1) + Z(-q_2) \to h^0(k_1) + h^0(k_2)$ process can be written as

$$\begin{aligned}
\mathcal{M}^{\mu\nu}_{ZZ} &= i\sqrt{2}G_F M_Z^2 \left\{ g^{\mu\nu} \left[2 + 4\sin^2(\beta-\alpha) \left(\frac{M_Z^2}{(q_1+k_1)^2 - M_Z^2} + \frac{M_Z^2}{(q_1+k_2)^2 - M_Z^2} \right) \right.\right. \\
&+ \frac{6\sin(\beta-\alpha)\left(2\cos(\beta+\alpha) + \sin 2\alpha \sin(\beta-\alpha)\right)}{\sin 2\beta} \frac{m_{h^0}^2}{(q_1+q_2)^2 - m_{h^0}^2} \\
&\left.\left. + \frac{2\cos^2(\beta-\alpha)\sin 2\alpha}{\sin 2\beta} \frac{m_{H^0}^2 + 2m_{h^0}^2}{(q_1+q_2)^2 - m_{H^0}^2} \right] \right. \\
&+ (q_1+2k_1)^\mu (q_2+2k_2)^\nu \left[\frac{\cos^2(\beta-\alpha)}{(q_1+k_1)^2 - m_{A^0}^2} + \frac{\sin^2(\beta-\alpha)}{(q_1+k_1)^2 - M_Z^2} \right] \\
&\left. + (q_1+2k_2)^\mu (q_2+2k_1)^\nu \left[\frac{\cos^2(\beta-\alpha)}{(q_1+k_2)^2 - m_{A^0}^2} + \frac{\sin^2(\beta-\alpha)}{(q_1+k_2)^2 - M_Z^2} \right] \right\}. \qquad \text{(B.1)}
\end{aligned}$$

For the $W^+(-q_1) + W^-(-q_2) \to h^0(k_1) + h^0(k_2)$ process, the matrix element is expressed as

$$\begin{aligned}
\mathcal{M}^{\mu\nu}_{W^+W^-} &= i\sqrt{2}G_F M_W^2 \left\{ g^{\mu\nu} \left[2 + 4\sin^2(\beta-\alpha) \left(\frac{M_W^2}{(q_1+k_1)^2 - M_W^2} + \frac{M_W^2}{(q_1+k_2)^2 - M_W^2} \right) \right.\right. \\
&+ \frac{6\sin(\beta-\alpha)\left(2\cos(\beta+\alpha) + \sin 2\alpha \sin(\beta-\alpha)\right)}{\sin 2\beta} \frac{m_{h^0}^2}{(q_1+q_2)^2 - m_{h^0}^2} \\
&\left.\left. + \frac{2\cos^2(\beta-\alpha)\sin 2\alpha}{\sin 2\beta} \frac{m_{H^0}^2 + 2m_{h^0}^2}{(q_1+q_2)^2 - m_{H^0}^2} \right] \right. \\
&+ (q_1+2k_1)^\mu (q_2+2k_2)^\nu \left[\frac{\cos^2(\beta-\alpha)}{(q_1+k_1)^2 - m_{H^\pm}^2} + \frac{\sin^2(\beta-\alpha)}{(q_1+k_1)^2 - M_W^2} \right] \\
&\left. + (q_1+2k_2)^\mu (q_2+2k_1)^\nu \left[\frac{\cos^2(\beta-\alpha)}{(q_1+k_2)^2 - m_{H^\pm}^2} + \frac{\sin^2(\beta-\alpha)}{(q_1+k_2)^2 - M_W^2} \right] \right\}. \qquad \text{(B.2)}
\end{aligned}$$

For the $W^-(-q_1) + W^+(-q_2) \to h^0(k_1) + h^0(k_2)$ process, we have $\mathcal{M}^{\mu\nu}_{W^-W^+} = \mathcal{M}^{\mu\nu}_{W^+W^-}$. In the region of $m_{H^0} > 2m_{h^0}$, the complex pole scheme is applied.

References

[1] G. Aad *et. al.* (ATLAS Collaboration), Phys. Lett. B **716**, 1 (2012).

[2] S. Chatrchyan *et. al.* (CMS Collaboration), Phys. Lett. B **716**, 30 (2012).

[3] CMS Collaboration, Report No. CMS-PAS-HIG-13-005.

[4] ATLAS Collaboration, Report No. ATLAS-CONF-2013-040.

[5] J.F. Gunion, H.E. Haber, G.L. Kane, and S. Dawson, Front. Phys. **80**, 1 (2000); J.F. Gunion, H.E. Haber, G.L. Kane, and S. Dawson, arXiv:hep-ph/9302272.

[6] G.C. Branco, P.M. Ferreira, L. Lavoura, M.N. Rebelo, M. Sher, and J.P. Silva, Phys. Rep. **516**, 1 (2012).

[7] M. Moretti, S. Moretti, F. Piccinini, R. Pittau, and A.D. Polosa, J. High Energy Phys. 02 (2005) 024.

[8] J. Baglio, A. Djouadi, R. Grober, M.M. Muhlleitner, J. Quevillon, and M. Spira, J. High Energy Phys. 04 (2013) 151; M.J. Dolan, C. Englert, and M. Spannowsky, J. High Energy Phys. 10 (2012) 112; A.J. Barr, M.J. Dolan, C. Englert, and M. Spannowsky, Phys. Lett. B **728**, 308 (2014); M.J. Dolan, C. Englert, N. Greiner, and M. Spannowsky, arXiv:1310.1084; F. Goertz, A. Papaefstathiou, L.-L. Yang, and J. Zurita, J. High Energy Phys. 06 (2013) 016.

[9] T. Han, G. Valencia, and S. Willenbrock, Phys. Rev. Lett. **69**, 3274 (1992).

[10] A. Djouadi and M. Spira, Phys. Rev. D **62**, 014004 (2000).

[11] A. Djouadi, W. Kilian, M. Muhlleitner, and P.M. Zerwas, Eur. Phys. J. C **10**, 45 (1999); R. Frederix, *et at.* arXiv:1401.7340.

[12] P. Bolzoni, F. Maltoni, S.O. Moch, and M. Zaro, Phys. Rev. Lett. **105**, 011801 (2010).

[13] P. Bolzoni, F. Maltoni, S.O. Moch, and M. Zaro, Phys. Rev. D **85**, 035002 (2012).

[14] L.-S. Ling, R.-Y. Zhang, W.-G. Ma, L. Guo, W.-H. Li, and X.-Z. Li, arXiv:1401.7754.

[15] M. Moretti, S. Moretti, F. Piccinini, R. Pittau, and J. Rathsman, J. High Energy Phys. 12 (2007) 075.

[16] T. Figy, Mod. Phys. Lett. A **23**, 1961 (2008).

[17] B. Coleppa, F. Kling, and S.-F. Su, arXiv:1305.0002.

[18] D. Eriksson, J. Rathsman, and O. Stal, Comput. Phys. Commun. **181**, 189 (2010).

[19] T. Hahn, Comput. Phys. Commun. **140**, 418 (2001).

[20] R. Mertig, M. Bohm, A. Denner, Comput. Phys. Commun. **64**, 345 (1991).

[21] W.L. van Neerven and A. Vogt, Nucl. Phys. **B568**, 263 (2000).

[22] S. Moch and J. Vermaseren, Nucl. Phys. **B573**, 853 (2000).

[23] W.L. van Neerven and A. Vogt, Nucl. Phys. **B588**, 345 (2000).

[24] J. Vermaseren, A. Vogt, and S. Moch, Nucl. Phys. **B724**, 3 (2005).

[25] S. Moch, J. Vermaseren, and A. Vogt, Nucl. Phys. **B813**, 220 (2009).

[26] E. Remiddi and J. Vermaseren, Int. J. Mod. Phys. A **15**, 725 (2000).

[27] T. Gehrmann and E. Remiddi, Comput. Phys. Commun. **141**, 296 (2001).

[28] A. Martin, W. Stirling, R. Thorne, and G. Watt, Eur. Phys. J. C **63**, 189 (2009).

[29] A. Martin, W. Stirling, R. Thorne, and G. Watt, Eur. Phys. J. C **64**, 653 (2009).

[30] T. Figy and D. Zeppenfeld, Phys. Lett. B **591**, 297 (2004).